



THE UNIVERSITY *of* EDINBURGH

Edinburgh Research Explorer

Photosensitizer doped zeolitic imidazolate framework-8 nanocomposites for combined antibacterial therapy to overcome methicillin-resistant *Staphylococcus aureus* (MRSA)

Citation for published version:

Li, J, Gopal, A, Karaosmanoglu, S, Lin, J, Munshi, T, Zhang, W, Chen, X & Yan, L 2020, 'Photosensitizer doped zeolitic imidazolate framework-8 nanocomposites for combined antibacterial therapy to overcome methicillin-resistant *Staphylococcus aureus* (MRSA)', *Colloids and Surfaces B: Biointerfaces*, vol. 190, 110900. <https://doi.org/10.1016/j.colsurfb.2020.110900>

Digital Object Identifier (DOI):

[10.1016/j.colsurfb.2020.110900](https://doi.org/10.1016/j.colsurfb.2020.110900)

Link:

[Link to publication record in Edinburgh Research Explorer](#)

Document Version:

Peer reviewed version

Published In:

Colloids and Surfaces B: Biointerfaces

General rights

Copyright for the publications made accessible via the Edinburgh Research Explorer is retained by the author(s) and / or other copyright owners and it is a condition of accessing these publications that users recognise and abide by the legal requirements associated with these rights.

Take down policy

The University of Edinburgh has made every reasonable effort to ensure that Edinburgh Research Explorer content complies with UK legislation. If you believe that the public display of this file breaches copyright please contact openaccess@ed.ac.uk providing details, and we will remove access to the work immediately and investigate your claim.



1 **Photosensitizer doped zeolitic imidazolate framework-8 nanocomposites for combined**
2 **antibacterial therapy to overcome methicillin-resistant *Staphylococcus aureus* (MRSA)**

3
4 Juan Li,[†] Ashna Gopal,[‡] Sena Karaosmanoglu,[‡] Jiafu Lin,[†] Tasnim Munshi,[°] Wenjun Zhang,^{*,§}
5 Xianfeng Chen,^{*,‡} and Li Yan^{*,†,§,||}

6
7 [†] Antibiotics Research and Re-evaluation Key Laboratory of Sichuan Province, Sichuan
8 Industrial Institute of Antibiotics (SIIA), Chengdu University, Chengdu, 610052, Sichuan, P.R.
9 China.

10
11 [‡] School of Engineering, Institute for Bioengineering, The University of Edinburgh, King's
12 Buildings, Mayfield Road, Edinburgh EH9 3JL, UK.

13
14 [§] Department of Materials Science and Engineering and Centre of Super Diamond & Advanced
15 Film (COSDAF), City University of Hong Kong, Hong Kong SAR

16
17 [°] School of Chemistry, University of Lincoln, Brayford Pool, Lincoln, Lincolnshire, LN6 7TS,
18 UK

19
20
21 **Corresponding Authors**

22 *Emails: tony_yan8@hotmail.com or tony.yan@monash.edu (L. Yan) Current Address:
23 Monash Institute of Pharmaceutical Sciences, Monash University, Parkville, Victoria 3052,
24 Australia, xianfeng.chen@oxon.org or Michael.Chen@ed.ac.uk (X. Chen) and
25 apwjzh@cityu.edu.hk (W.J. Zhang)

26
27 The total number of words of the manuscript, including entire text from title page to figure
28 legends: 5196

29 The number of words of the abstract: 109

30 The number of figures: 7

31 The number of tables: 0

32

33 **Abstract**

34 Antibiotics have played an important role in the treatment of bacteria related infections.
35 However, the rapid emergence of multidrug-resistant bacteria and limited number of antibiotics
36 available is a great challenge to humankind. To circumvent the use of antibiotics and hence,
37 address this problem, we are proposing a photosensitizer-modified biodegradable zeolitic
38 imidazolate framework-8 nanocomposite that can kill not only Gram-positive bacteria
39 *Staphylococcus aureus*, but also methicillin-resistant *Staphylococcus aureus* with high efficacy.
40 *In vivo* testing revealed that these nanocomposites are highly effective for *in vivo* wound
41 disinfection with minimal side-effects. In conclusion, this photosensitizer-modified
42 biodegradable nanocomposite could be very promising for a synergistic antibacterial therapy to
43 overcome methicillin-resistant *Staphylococcus aureus* (MRSA).

44 **Keywords:** zeolitic imidazolate framework 8; photosensitizer; photodynamic therapy;
45 antibacterial therapy
46

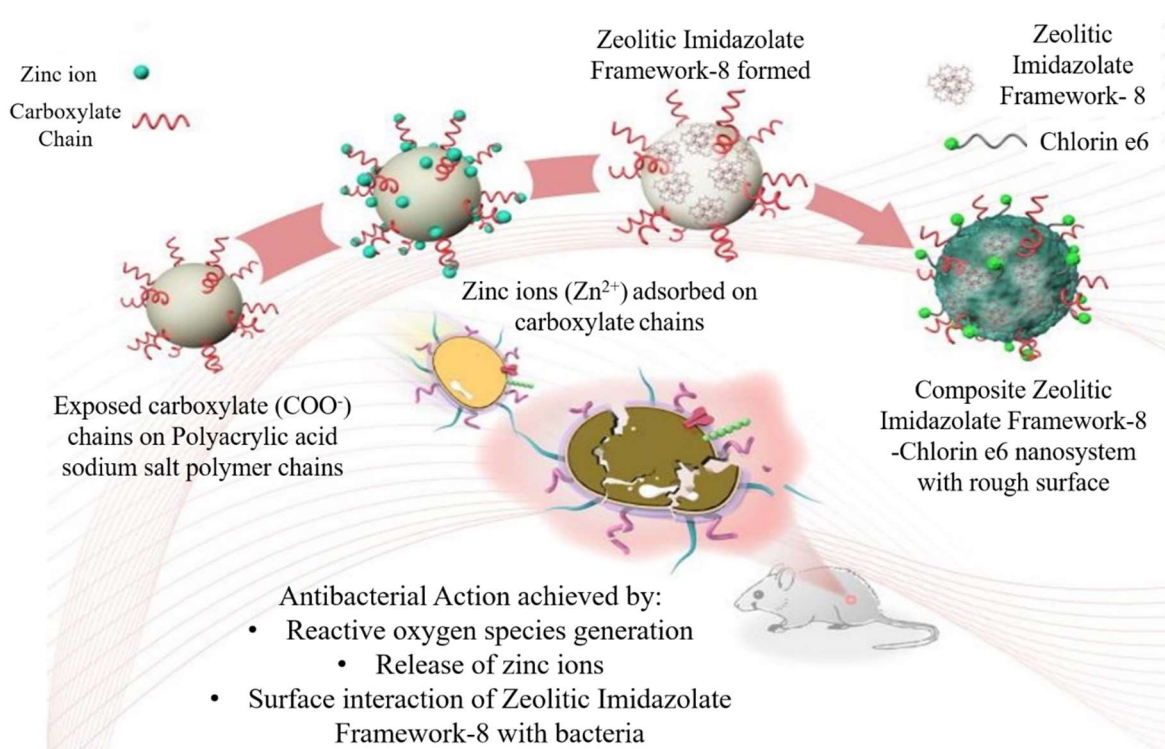
47 48 **1. Introduction**

49 Bacterial infection is one of the most prominent causes of serious diseases¹⁻³. The wide
50 range and biological variations of pathogenic microorganisms often lead to great
51 challenges in antimicrobial treatment in clinical settings. With the discovery and
52 development of antibiotics, the treatment of bacterial infection has been revolutionised⁴
53⁵. However, long-term abuse and overdose of antibiotics have led to bacterial cells
54 adversely modifying antibiotic molecules, thereby leading to the emergence of drug-
55 resistant bacteria⁶⁻⁷. This, in turn, poses a serious public health threat that contributes to
56 millions of severe infections and even thousands of deaths every year⁸. According to the
57 World Health Organisation, more than 700,000 people die worldwide every year from
58 antibiotic resistant infections and this figure is expected to rise to 10 million a year by
59 2050⁹. Although great efforts have been dedicated to creating new and more effective

60 antibiotics, the rate of antibiotic development is still far more behind the high evolution
61 rate of pathogenic microorganisms. An example is methicillin-resistant *Staphylococcus*
62 *aureus* (MRSA), which was first discovered in England and is considered as one of the
63 most dangerous clinical pathogens (often known as ‘superbugs’) causing life-threatening
64 diseases¹⁰. Thus, it is crucial that new antimicrobial agents and methods are developed
65 to mitigate the persistent issue of drug tolerance. One potential solution is to use
66 nanomaterials for the delivery of antimicrobial agents. The ability of nanomaterials to
67 allow enhanced localization to bacteria as well as tunable interaction with bacteria upon
68 surface modification with different charges, roughness, and functional groups can
69 greatly improve therapeutic properties and efficiency¹¹. Among nanomaterials, metal-
70 organic frameworks (MOFs) have been developed for many biomedical applications<sup>12-
71 16</sup>. MOFs are constructed using metal ions and organic linker molecules to form
72 nanoporous materials with many advantages including high surface area, tunable pore
73 size and porosity, high drug loading capacity, good biocompatibility, potential
74 biodegradability, and greater flexibility in the selection of organic and inorganic
75 components¹⁷⁻¹⁹. Therefore, several MOFs with different functionalities have been
76 successfully designed for antibiotic and silver loading for increased antibacterial
77 efficacy²⁰⁻²². Liu and co-workers have reported the use of MIL-100 (Fe) MOFs as a
78 nanocarrier to deliver the metabolic labelling molecule 3-azido-D-alanine for precise
79 bacterial detection and fluorescence image-guided therapy²³. Beyond these applications
80 of using MOFs, we herein propose an integrated multifunctional nano MOF (NMOFs)
81 system based on zeolitic imidazolate framework-8 (ZIF-8) for antibacterial applications
82 (**Figure 1**). Photodynamic therapy (PDT) is widely utilized for biomedical applications
83 including cancer therapy, wound healing and disinfection.²⁴⁻²⁶ This technique makes use
84 of light excitation to generate reactive oxygen species (ROS) to directly attack and kill
85 pathogenic microorganisms²⁷⁻²⁸. The ROS reacts with diverse bioactive molecules in

86 pathogenic bacteria and its generation has been found to be very promising in the
 87 endeavour to solve the antibiotic resistance problem²⁹. To achieve a nanocomposite
 88 capable of photodynamic therapy, the photosensitiser, Chlorin e6 (Ce6) was chosen
 89 because of its low dark toxicity and high efficacy. Furthermore, Ce6 was selected over
 90 other photosensitising drugs as it can be easily attached on the surface of the ZIF-8 via
 91 an intermediate conjugation step with APTES and then mixing with the ZIF-8 solution.
 92 Secondly, in our proposed hybrid structure, the Zn^{2+} ions act as a toxin for the inhibition
 93 of bacterial growth³⁰. Third, the nanoparticles possess a rough surface which has been
 94 demonstrated to drastically influence the interaction with bacterial cells, thereby
 95 achieving high antibacterial efficacy³¹⁻³³. Finally, the soft-template based NMOFs are
 96 pH-sensitive and easily decompose in a weak acid environment compared to other
 97 nanocomposites such as silica and zinc oxides nanoparticles.

98



99
 100
 101
 102
 103

Figure 1. Schematic illustration of Ce6 doped ZIF-8 nanoparticles fabrication and their use for photo-inspired disinfection.

104 **2. EXPERIMENTAL SECTION**

105 **2.1 Chemicals and Characterization.** 1-Ethyl-3-(3-dimethylaminopropyl) carbodiimide
106 (EDC), 2-methylimidazole (linker) and 1, 3-diphenylisobenzofuran (DPBF) were purchased
107 from Damas-beta. Zinc nitrate hexahydrate ($\text{Zn}(\text{NO}_3)_2 \cdot 6\text{H}_2\text{O}$) and poly(acrylic acid, sodium
108 salt) (PAAS) were from Strem and Sigma-Aldrich, respectively. Methyl alcohol, ethyl alcohol,
109 isopropyl alcohol and absolute ethyl alcohol, were purchased from General-Reagent, China. (3-
110 aminopropyl) triethoxysilane (APTES) and Chlorin e6 (Ce6) were ordered from J&K and
111 Frontier Scientific, respectively. Transmission electron microscopy (TEM) images were taken
112 on a Tecnai G2 F20 S-TWIN. The UV–VIS absorption spectrum was determined with a UV-
113 1900PC UV–visible spectrophotometer. Powder X-ray diffraction (XRD) patterns, Fourier
114 transform infrared spectroscopy (FT-IR) and X-ray photoelectron spectroscopy (XPS) were
115 recorded using a BRUKER D8 instrument with Cu $K\alpha$ radiation, Nicolet IS10 and Thermo
116 escalab 250Xi, respectively. The L13152 Invitrogen™ Molecular Probes™ LIVE/DEAD®
117 BacLight Bacterial Viability Kit was obtained from Thermo Fisher Scientific.

118 **2.2 Preparation of APTES Conjugated Ce6.** 1 mg of Ce6 and 20 μL of APTES were added
119 to 1 mL of ethyl alcohol in the presence of EDC as a catalyst and magnetically stirred for 24 h
120 at room temperature.

121 **2.3 Preparation of ZIF-8 and Ce6 doped ZIF-8.** First, 50 μL of 200 $\mu\text{g}/\text{mL}$ PAAS were added
122 to 1.5 mL of H_2O , then 6 mL of isopropyl alcohol was added in a dropwise manner. 0.1M Zn^{2+}
123 solution was prepared by dissolving $\text{Zn}(\text{NO}_3)_2 \cdot 6\text{H}_2\text{O}$ in methyl alcohol and 1.25 mL of the 0.1
124 M Zn^{2+} was quickly added to the liquid mixture and stirred for 5 min at room temperature. 2.5
125 mL of 20 mg/mL 2-methylimidazole dissolved in methyl alcohol was then injected into the
126 mixture and kept stirring for 4 h at 60°C. The solution was subsequently cooled and precipitated
127 by centrifugation at 6000 rpm for 10 min. The resulting solid was washed with absolute ethyl
128 alcohol and water thrice. The sediment was then dispersed into 5 mL of 50% ethyl alcohol.
129 Next, the APTES conjugated Ce6 was added to the solution and kept stirring for an additional

130 24 h. After the reaction, the product was washed with ethyl alcohol and water thrice and then
131 dried in a vacuum to yield Ce6 doped ZIF-8.

132 **2.4 Singlet Oxygen Generation Ability Analysis.** 2.82 mL of 0.05 mg/mL DPBF solution in
133 dimethyl sulfoxide (DMSO) was added into a quartz colorimetric dish. 0.18 mL of free Ce6 or
134 Ce6 doped ZIF-8 containing 900 ng of Ce6 was added to different individual dishes. The dishes
135 were then irradiated with a 650 nm LED lamp. After irradiation, the absorbance of the sample
136 in each dish was measured at 410 nm using a UV-1900PC UV-visible spectrophotometer.

137 **2.5 Antibacterial Test.** *Staphylococcus aureus* (*S. aureus*) and MRSA were chosen as bacterial
138 models to evaluate the antibacterial activity. The bacterial concentration in Lysogeny broth
139 (LB) was maintained at about 10^6 CFU mL⁻¹ and cultured at 37°C in an incubator-shaker.
140 Corning 96-well plates were used for this test. Four pre-determined concentrations of
141 nanoparticles were prepared in milli-Q water and these were added to the bacterial suspension
142 in a 1:1 ratio and then incubated. For the groups being treated with light, the Corning 96-well
143 plates were exposed to 650 nm LED light for 30 minutes at an intensity of 150 (100x LUX)
144 before incubation at 37 °C for 12 h. The bacterial inhibition growth curve was determined by
145 measuring the optical density at 600 nm at 2 h time intervals over the 12-h period.

146 **2.6 Live-Dead Imaging.** The antibacterial effect of Ce6-doped ZIF-8 nanoparticles and LED
147 light irradiation were demonstrated using Live/Dead Imaging. *Staphylococcus Aureus* was used
148 as the model bacteria. Four treatment groups were considered namely, bacteria without light
149 irradiation (A), bacteria with light irradiation (B), nanoparticles treated with bacteria but
150 without light irradiation (C) and nanoparticles treated with bacteria with light irradiation (D).
151 10 µL from a *Staphylococcus Aureus* (USA300) stock was cultured overnight on LB agar at
152 37°C for 18 h. A single colony was then inoculated in liquid LB media and grown overnight at
153 37 °C with shaking at 200 rpm. The overnight culture was then diluted (1:100) and the sample
154 incubated until an optical density of ~0.5 at 600 nm was reached. PBS was then used to wash
155 the culture by centrifugation at 5000 rpm for 5 minutes at 4 °C and resuspension. Fresh liquid

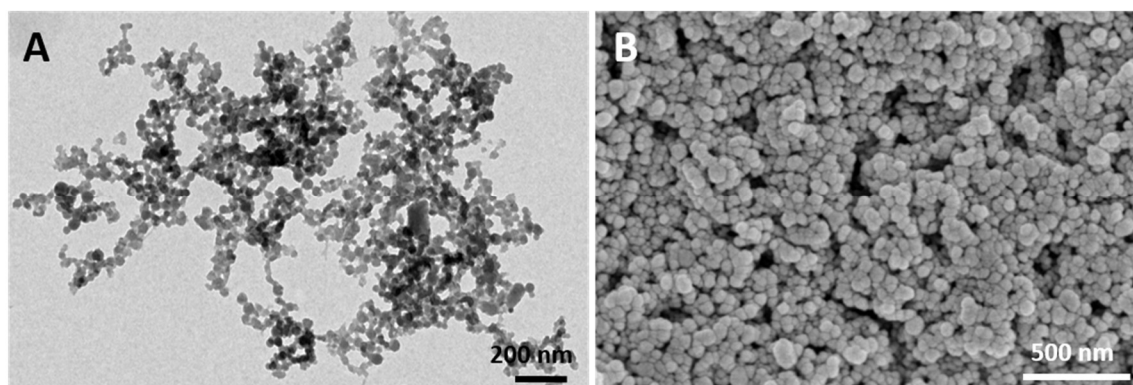
156 media was added to the bacteria and then serially diluted to adjust the optical density to 0.05
157 ($\sim 10^6$ CFU mL⁻¹). A stock solution of the Ce6-doped ZIF-8 nanoparticles dispersed in milli-Q
158 water was prepared at a concentration of 1 mg/mL. Then, a 5 mL solution with a concentration
159 of 22.2 μ g/mL from this stock solution was prepared and sonicated for 20 mins for an even
160 nanoparticle dispersion. 1 mL of this solution was added to 1 mL of the bacterial culture (for
161 conditions C and D) in a sterile 6-well plate. The bacterial suspension for conditions A and B
162 were left untreated and 1 mL of PBS was added as a control. The plate was then incubated at
163 37°C for 2 hours in the dark with shaking. After 2 hours, the wells containing bacteria from
164 conditions B and D were exposed to a 650 nm LED light source for 30 minutes placed at a
165 vertical height of 22 cm from the plate. The plate was then further incubated for 2 hours at 37°C
166 with shaking. After incubation, a 1:1000 dilution was carried out with each of the four samples
167 and 100 μ L of the diluted solution was plated for CFU determination. The remaining solution
168 in each well was transferred into 2 mL Eppendorf tubes, washed thrice with PBS by
169 centrifugation at 15000 rpm for 5 mins and then re-suspended in 500 μ L of PBS. The four
170 samples were then stained by adding an equal amount of PI/Syto9 dye mixture prepared as per
171 the manufacturer's instructions. The stained bacterial suspensions were then incubated in the
172 dark for 15 minutes. To remove excess dye, each sample was washed with PBS thrice by
173 centrifugation at 20000 rpm for 5 mins and then finally resuspended in 200 μ L of PBS. 20 μ L
174 of each of this stained bacterial suspension was trapped between a slide and a 25 mm diameter
175 round coverslip. The edges of the coverslip were sealed, and the samples observed in a Zeiss
176 LSM 880 with Fast Airyscan confocal microscope.

177 **2.7 Animal Wound Infection Model and Histological Analysis.** All the procedures were
178 carried out in accordance with the guidelines issued by Chengdu University and Sichuan
179 Province. All the experiments were approved by the Animal Ethics Committee of Chengdu
180 University. Four groups of mice were randomly divided. A wound of about 6 mm² was

181 developed at the dorsal side of each mouse. After 24 h, the wounds were infected with *S. aureus*
182 and then treated with the Ce6 doped ZIF-8 nanoparticles. The light treated group of mice was
183 exposed to 650 nm LED light for 30 mins. At day 17, all mice were sacrificed. The heart, liver,
184 spleen, lung, kidney, and wound were harvested and the tissues fixed in a 10% formalin solution,
185 embedded in paraffin, sectioned, and stained. All the samples were subsequently processed for
186 hematoxylin and eosin (H&E) staining.

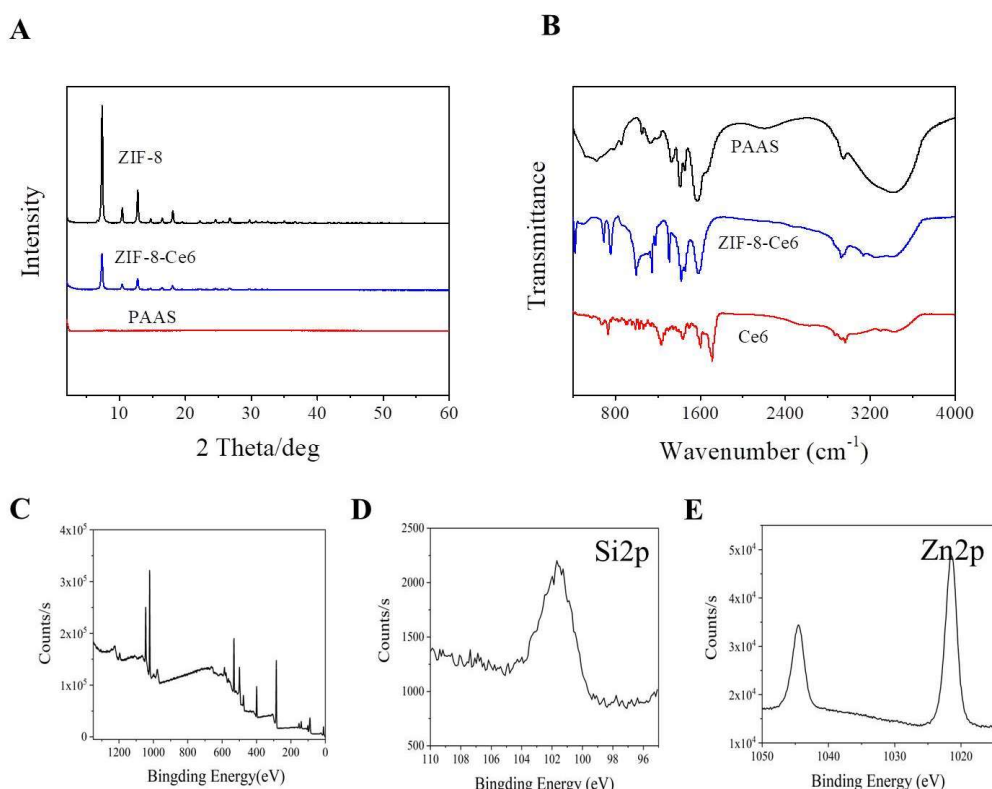
187 3. RESULTS AND DISCUSSION

188 Nanoscale ZIF-8 was fabricated using poly(acrylic acid sodium salt) (PAAS) nanosphere as a
189 soft template.³⁴⁻³⁵ Since Zn^{2+} has a higher affinity towards the $-COO^-$ group in the PAAS
190 polymer chain, it was absorbed on the PAAS and thus, replaced the Na^+ . Then, 2-
191 methylimidazole (2-MIMs) was added and reacted with the Zn^{2+} on the surface to form ZIF-8
192 nanocrystal on the PAA nanosphere. Next, (3-aminopropyl) triethoxysilane (APTES)
193 conjugated Ce6 was reacted with the nanocomposite for drug conjugation. The ZIF-8
194 nanocomposite has a diameter of approximately 50-90 nm and (**Figure 2** and Figure S1) the
195 Ce6 loading in the nanocomposite is 4.5 wt% (Figure 2 and Figure S1). As illustrated in **Figure**
196 **3A**, the fabricated nanocomposite has XRD peaks identical to ZIF-8, confirming successful
197 formation of ZIF-8 crystal structure. The Fourier transform infrared (FT-IR) spectrum of the
198 nanocomposite contains Ce6 peaks, establishing the successful conjugation of Ce6 (Figure 3B).
199 In addition, the X-ray photoelectron spectroscopy (XPS) confirms the existence of Zn and Si
200 elements in the nanoparticles with a weight atomic ratio of 8.58% and 4.11%, respectively.
201 (Figure 3C-E and Table S1)



202
203
204
205

Figure 2. Characterisation of Ce6 doped ZIF-8 nanoparticles: A. TEM image and B. SEM image.

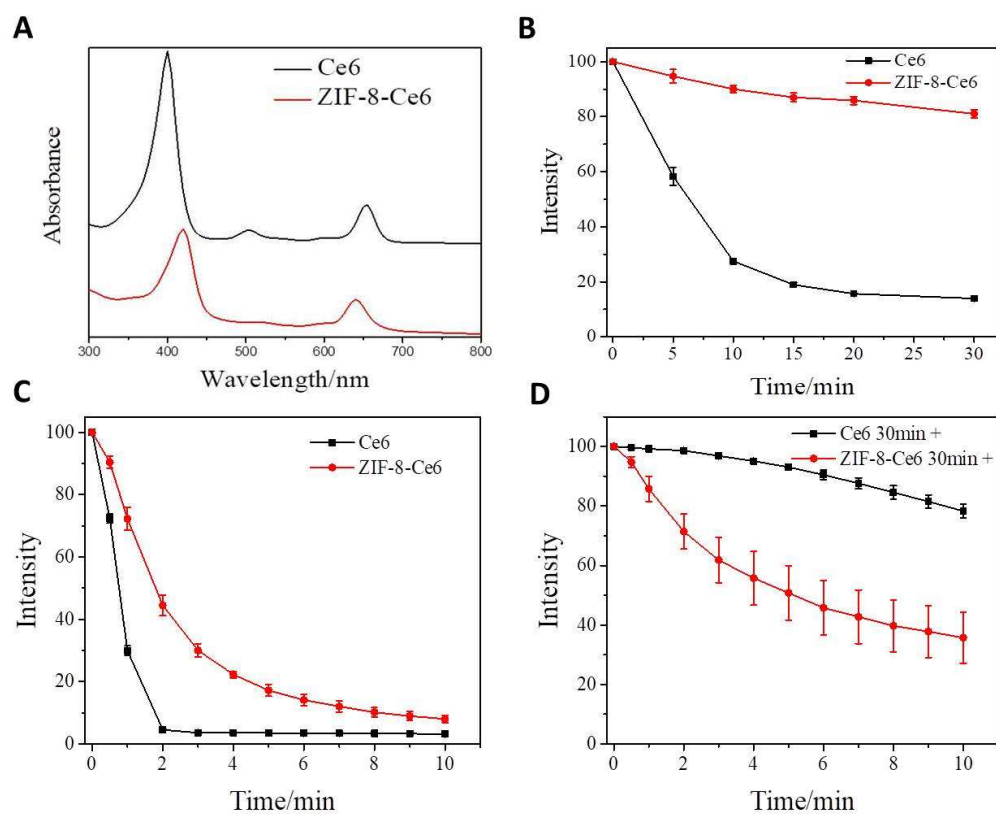


206
207
208
209
210
211

Figure 3 A. Powder X-Ray diffraction pattern, B. Fourier transform infrared spectroscopy and C. XPS analysis of Ce6 doped ZIF-8 nanoparticles.

211 Next, the optical properties of the Ce6 doped ZIF-8 were evaluated. **Figure 4A** shows the
212 absorbance spectra of Ce6 doped ZIF-8 nanocomposite and free Ce6 molecules, it is apparent
213 that the spectra are similar but with a shift in absorbance of the peaks. We then investigated the
214 photo-stability of the Ce6 doped ZIF-8 when exposed to light (Figure 4B and Figure S2), it was
215 found that the absorbance intensity of free Ce6 molecules dramatically decreases after a short
216 period of light exposure. In contrast, the absorbance intensity of Ce6 doped ZIF-8

217 nanocomposite is much more stable. Next, a fluorescence probe, 1, 3-diphenylisobenzofuran
218 (DPBF), was used to detect singlet oxygen molecules and study the ROS generation capacity
219 of the Ce6 doped ZIF-8 nanoparticles. Under 650 nm LED light irradiation, both free Ce6
220 molecules and Ce6 doped ZIF-8 can effectively generate singlet oxygen (Figure 4C). To further
221 study the photo-stability of the Ce6 doped ZIF-8 nanocomposites, their ROS generation
222 capacity was investigated after light exposure. Both Ce6 doped ZIF-8 and Ce6 molecules were
223 initially exposed to 650 nm LED light for 30 minutes and then the formation of ROS from each
224 material was studied. As presented in Figure 4D, free Ce6 molecules lose the majority of their
225 ROS generation capacity after light exposure as indicated by the small decrease in rate of the
226 absorbance of DPBF, while the Ce6 doped ZIF-8 can still generate ROS, thereby resulting in a
227 substantial decrease of the absorbance of DPBF. Next, we tested the biodegradability of
228 fabricated Ce6 doped nanoscale ZIF-8 in a weak acid environment. As shown in Figure S3, the
229 nanocomposite is biodegradable in a weak acid environment and loses its whole structure within
230 6 hours in a pH 5 environment.

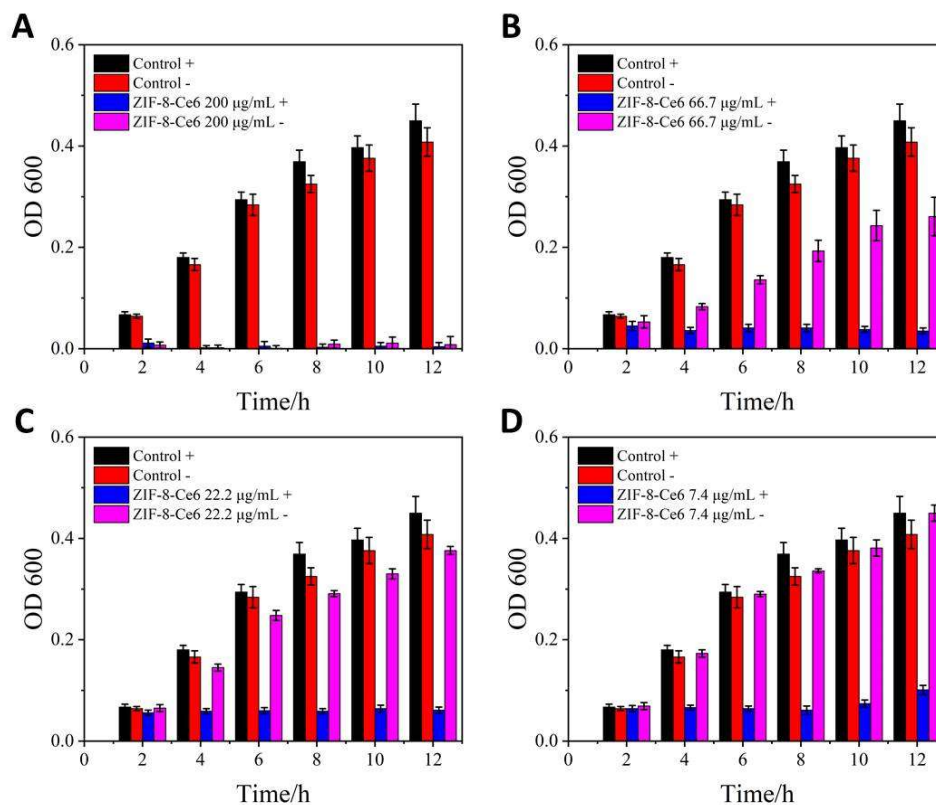


231

232
233 **Figure 4.** Optical properties and singlet oxygen generation capacity of Ce6 doped ZIF-8
234 nanoparticles. A. Absorption spectra of Ce6 doped ZIF-8 and free Ce6 molecules. B.
235 Normalized 400 nm absorbance intensity change of Ce6 doped silica and free Ce6 caused by
236 650 nm LED irradiation. C-D. Absorbance spectra of DPBF with the addition of Ce6 doped
237 silica and free Ce6 under LED illumination. (C) Degradation in intensity when DPBF added
238 with Ce6 doped silica and free Ce6, (D) Degradation in intensity when Ce6 doped silica and
239 free Ce6 were illuminated under 650 nm LED light for 30 min before addition of DPBF. Data
240 in B-D are expressed as mean \pm s.d. (indicated by error bars), based on values obtained from
241 three replicates (n=3).
242

243 The antibacterial performance of Ce6 doped ZIF-8 was subsequently analyzed with *S. aureus*
244 and MRSA as model bacteria (Figure S4 and **Figure 5**). The growth of bacteria in liquid media
245 was monitored by measuring the optical density of Luria-Bertani (LB) broth at a wavelength of
246 600 nm. At first, the influence of light irradiation on bacterial growth was excluded by
247 comparing the growth of bacteria with and without light illumination. It was found that the
248 bacterial growth with and without light illumination was nearly identical, suggesting that the
249 light at the used power does not inhibit bacteria growth. At a concentration of 200 $\mu\text{g/mL}$, the
250 Ce6 doped ZIF-8 nanoparticles could effectively inhibit the growth of *S. aureus* and MRSA
251 irrespective of light illumination. This indicates that the Ce6 doped ZIF-8 nanoparticles are
252 toxic to bacteria; the toxicity originates from the Zn^{2+} ions within the material, as Ce6 cannot
253 kill bacteria in the absence of light illumination. When the concentration was decreased to 66.7
254 $\mu\text{g/mL}$, the Ce6 doped ZIF-8 nanoparticles partially inhibited the growth of bacteria in the
255 absence of light irradiation. In comparison, Ce6 doped ZIF-8 nanoparticles at the same
256 concentration could effectively inhibit the growth of both MRSA and *S. aureus* upon light
257 irradiation. This demonstrates that the photo-toxicity of the Ce6 doped ZIF-8 is also responsible
258 for bacterial growth inhibition. To confirm this observation, we further dropped the
259 concentration of the Ce6 doped ZIF-8 nanocomposite to 22.2 and 7.4 $\mu\text{g/mL}$ and found that the
260 Ce6 doped ZIF-8 nanoparticles were still able to completely inhibit *S. aureus* and MRSA
261 growth in the presence of LED light. This finding was also confirmed when the plate count
262 method was used (Figure S5 and Figure S6). Results from a statistical t-test revealed a p-value

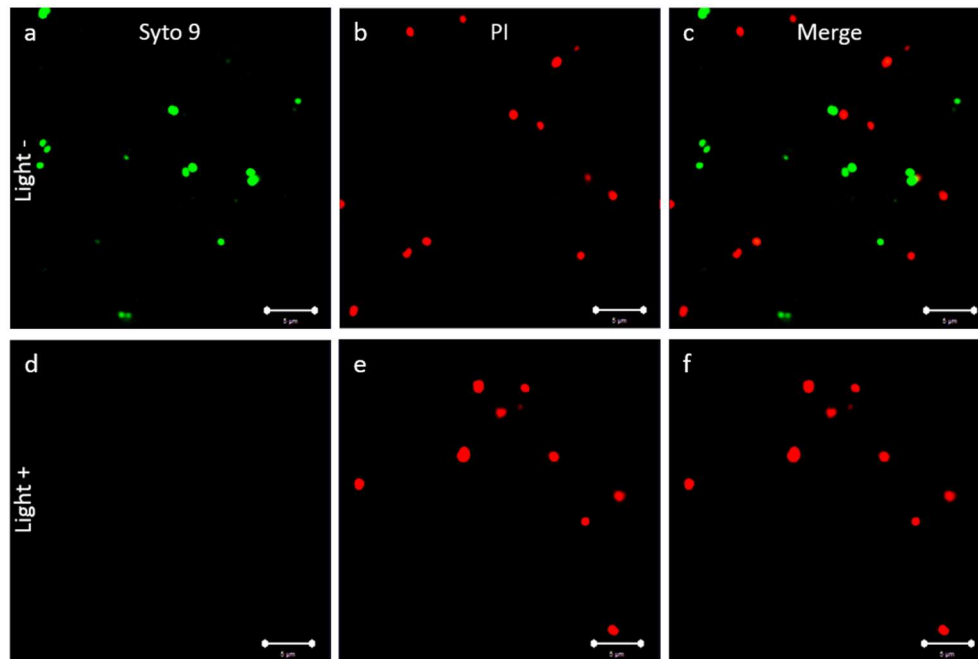
263 of $<<0.05$ which showed a significant difference between the ZIF-Ce6 nanoparticles and light
 264 group and any other group at the 12 h time point for all 4 tested concentrations. Overall, the
 265 Ce6 doped ZIF-8 nanoparticles exhibited excellent light-induced antibacterial performance.



266
 267 **Figure 5.** Anti-MRSA performance of Ce6 doped ZIF-8 with different concentrations: A. 200
 268 $\mu\text{g/mL}$, B. 66.7 $\mu\text{g/mL}$, C. 22.2 $\mu\text{g/mL}$ and D. 7.4 $\mu\text{g/mL}$. Control means only LB added. “+”
 269 indicates with light illumination; “-” indicates without light illumination. All data are expressed
 270 as mean \pm s.d. (indicated by error bars), based on values obtained from six biological replicates
 271 ($n=6$).

272 After demonstrating the antibacterial ability of Ce6-doped ZIF-8 nanoparticles by measuring
 273 the optical density and counting the CFU number of bacteria, we continued this investigation
 274 using confocal fluorescence microscopy imaging. We performed Live/Dead bacterial staining
 275 using the L13152 Invitrogen™ Molecular Probes™ BacLight™ Bacterial Viability Kit. The
 276 Syto9 dye stains bacteria with both intact membranes and damaged membranes while the
 277 propidium iodide dye penetrates only the bacteria with damaged membranes. As evidenced by
 278 the confocal images in **Figure 6**, a low concentration of Ce6-doped ZIF-8 nanoparticles (22.2
 279 $\mu\text{g/mL}$) alone is not enough to kill all bacterial cells; however, if bacteria are exposed to both

280 nanoparticles at the same concentration and light irradiation, nearly all bacteria are killed. This
281 is in line with the above results obtained by CFU plating and optical density measurements.
282 The synergistic effect shown in these experiments demonstrates the potent efficacy of the
283 proposed combined therapy and implies that nanoparticles at very low concentrations can still
284 yield effective antibacterial efficiency.

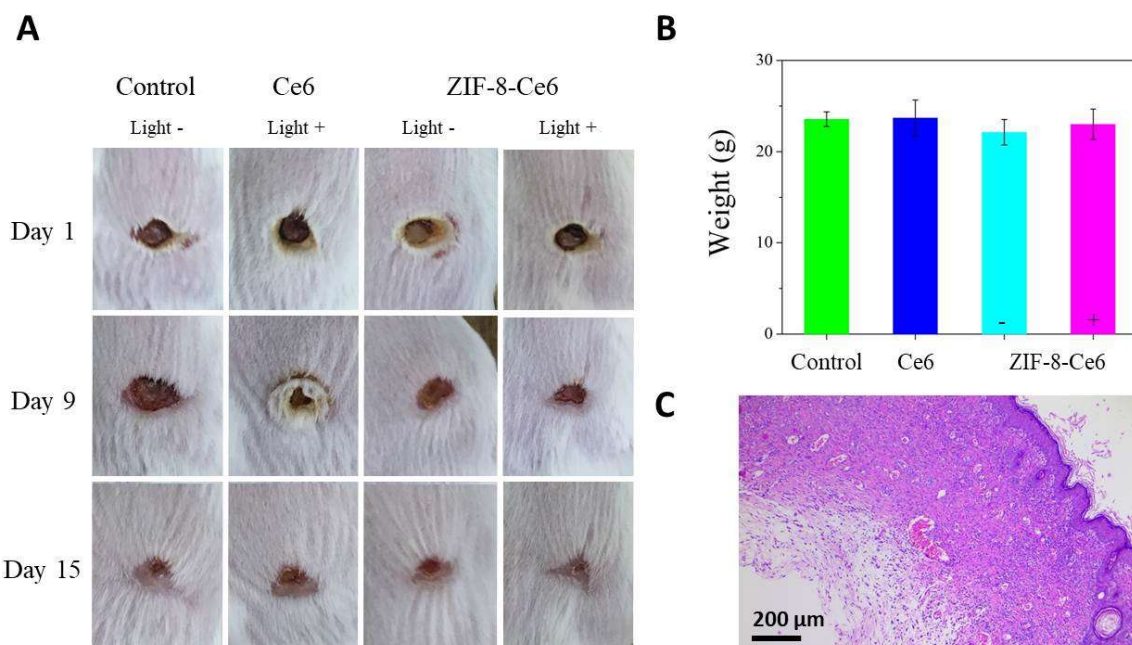


285

286 **Figure 6.** Live/dead staining of *S. aureus* treated with Ce6-doped ZIF-8 nanoparticles in the
287 absence of light (Light -) (a-c) and presence of light irradiation (light +) (d-f). Scale bars indicate
288 5 μm . The concentration of Ce6-doped ZIF-8 nanoparticles used for imaging was 22.2 $\mu\text{g/mL}$.
289

290 Finally, it is important to determine if this technique could be potentially used in clinical
291 applications. Thus, the *in vivo* anti-infection performance of Ce6 doped ZIF-8 nanoparticles
292 was evaluated using a Balb/c mouse model. A wound was created on the back of mice followed
293 by infection with *S. aureus* bacteria. (**Figure 7**) The mice were then randomly divided into four
294 groups. One group of mice was treated with free Ce6 molecules and irradiated with light. Two
295 groups of mice were treated with Ce6 doped ZIF-8 nanoparticles (one with light irradiation and
296 the other without light irradiation). Another group of mice were used as a control and not
297 subjected to any treatment. Figure 7A shows the digital images of wounds for each of the

298 different treatment conditions. A clear difference in wound morphology after treatment was
 299 observed. It is apparent that the wounds treated by the Ce6 doped ZIF-8 nanoparticles with light
 300 irradiation show a better recovery pattern than other groups. Wounds like the ones introduced
 301 in this experiment have a general tendency to be alkaline and slowly turn acidic as wound
 302 healing is initiated.³⁶ As the ZIF-8-Ce6 nanocomposites are responsive to acidic pH, their
 303 dissociation within the wound environment could enhance their antibacterial function while
 304 being finally cleared. Haematoxylin and Eosin (H&E) analysis of wound harvested from mice
 305 treated with both Ce6 doped ZIF-8 and light irradiation reveals a complete and intact skin
 306 structure. In addition, no obvious abnormality was found in the major organs of the mice treated
 307 with the Ce6 doped ZIF-8 nanoparticles and light irradiation.(Figure S7) During the whole
 308 experimental period, no obvious change in body weight was found in all groups (Figure 7B).
 309 Collectively, these observations demonstrate the robust wound healing efficiency and good
 310 biocompatibility of the synthesized Ce6-doped ZIF-8 nanoparticles.



311
 312 **Figure 7.** *In vivo* antibacterial evaluation of *S. aureus* infected wound treated with Ce6 doped
 313 ZIF-8. A. Digital images of *S. aureus* infected wound treated with different drug formations. B.
 314 Body weight of mice treated in different groups. Data are expressed as mean \pm s.d. (indicated
 315 by error bars). C. Haematoxylin and Eosin stain of *S. aureus* infected skin tissue sections treated
 316 with Ce6 doped rough silica with light irradiation.

317 **4. Conclusion**

318 In conclusion, our study illustrates a strategy for the synthesis of Ce6 doped ZIF-8
319 nanoparticles for enhanced antibacterial applications, with a strong potential for killing
320 bacteria with multi-drug resistance. The conjugation of Ce6 to ZIF-8 nanoparticles could
321 significantly improve the photostability and ROS generation capacity of free Ce6
322 molecules. Our *in vitro* testing and live/dead imaging demonstrates the excellent
323 synergistic therapeutic efficacy of the Ce6-doped ZIF-8 nanoparticles against *S. aureus*
324 and MRSA. The *in vivo* wound healing studies on *S. aureus* infected mice further
325 confirmed the highly effective antibacterial performance and good biocompatibility of
326 the nanoparticles and thus, warrants their future applications in clinical settings.

327 **Declaration of Interest**

328 -
329 -
330 -

331 **Appendix A. Supplementary data**

332
333 Supplementary material (SEM images, time-dependent morphology and absorbance changes,
334 bacterial colony-forming units, hematoxylin and eosin stain images) related to this article can
335 be found, in the online version, at doi:

336
337 **ACKNOWLEDGMENTS**

338
339 The authors acknowledge the support provided from National Natural Science Foundation of
340 China (No. 81803480), General Research Fund of Hong Kong (CityU Grant Nos. 11338516
341 and 11306717), the Royal Society Research Grant Scheme RG150564 and the Chengdu
342 University (Nos. 2081916010 and ARRLKF16-05).
343 J. Li and A. Gopal contributed equally to this work.

344
345 **REFERENCES**

- 346
347 1. Li, M.; Sultanbawa, Y.; Xu, Z. P.; Gu, W.; Chen, W.; Liu, J.; Qian, G., High and long-
348 term antibacterial activity against Escherichia coli via synergy between the antibiotic penicillin
349 G and its carrier ZnAl layered double hydroxide. *Colloids Surf. B Biointerfaces* **2019**, *174*, 435-
350 442. DOI: 10.1016/j.colsurfb.2018.11.035.
351 2. Chen, W.; Zhang, B.; Mahony, T.; Gu, W.; Rolfe, B.; Xu, Z. P., Efficient and Durable
352 Vaccine against Intimin beta of Diarrheagenic E. Coli Induced by Clay Nanoparticles. *Small*
353 **2016**, *12* (12), 1627-39. DOI: 10.1002/sml.201503359.

- 354 3. Zhang, M.; Wang, P.; Sun, H.; Wang, Z., Superhydrophobic surface with hierarchical
355 architecture and bimetallic composition for enhanced antibacterial activity. *ACS Appl. Mater.*
356 *Interfaces* **2014**, *6* (24), 22108-15. DOI: 10.1021/am505490w.
- 357 4. Li, Y.; Zhao, Z.; Zhang, J.; Kwok, R. T. K.; Xie, S.; Tang, R.; Jia, Y.; Yang, J.; Wang,
358 L.; Lam, J. W. Y.; Zheng, W.; Jiang, X.; Tang, B. Z., A Bifunctional Aggregation-Induced
359 Emission Luminogen for Monitoring and Killing of Multidrug-Resistant Bacteria. *Adv. Funct.*
360 *Mater.* **2018**, *28* (42), 1804632. DOI: 10.1002/adfm.201804632.
- 361 5. Klein, E. Y.; Van Boeckel, T. P.; Martinez, E. M.; Pant, S.; Gandra, S.; Levin, S. A.;
362 Goossens, H.; Laxminarayan, R., Global increase and geographic convergence in antibiotic
363 consumption between 2000 and 2015. *Proc. Natl. Acad. Sci.* **2018**, *115* (15), E3463. DOI:
364 10.1073/pnas.1717295115.
- 365 6. Li, X.; Bai, H.; Yang, Y.; Yoon, J.; Wang, S.; Zhang, X., Supramolecular Antibacterial
366 Materials for Combatting Antibiotic Resistance. *Adv. Mater.* **2019**, *31* (5), 1805092. DOI:
367 10.1002/adma.201805092.
- 368 7. Dai, X.; Zhao, Y.; Yu, Y.; Chen, X.; Wei, X.; Zhang, X.; Li, C., All-in-one NIR-
369 activated nanoplatfoms for enhanced bacterial biofilm eradication. *Nanoscale* **2018**, *10* (39),
370 18520-18530. DOI: 10.1039/C8NR04748K.
- 371 8. Linklater, D. P.; De Volder, M.; Baulin, V. A.; Werner, M.; Jessl, S.; Golozar, M.;
372 Maggini, L.; Rubanov, S.; Hanssen, E.; Juodkazis, S.; Ivanova, E. P., High Aspect Ratio
373 Nanostructures Kill Bacteria via Storage and Release of Mechanical Energy. *ACS Nano* **2018**,
374 *12* (7), 6657-6667. DOI: 10.1021/acsnano.8b01665.
- 375 9. Tagliabue, A.; Rappuoli, R., Changing Priorities in Vaccinology: Antibiotic Resistance
376 Moving to the Top. *Frontiers immunol.* **2018**, *9*, 1068-1068. DOI: 10.3389/fimmu.2018.01068.
- 377 10. Hu, D.; Li, H.; Wang, B.; Ye, Z.; Lei, W.; Jia, F.; Jin, Q.; Ren, K.-F.; Ji, J., Surface-
378 Adaptive Gold Nanoparticles with Effective Adherence and Enhanced Photothermal Ablation
379 of Methicillin-Resistant Staphylococcus aureus Biofilm. *ACS Nano* **2017**, *11* (9), 9330-9339.
380 DOI: 10.1021/acsnano.7b04731.
- 381 11. Armentano, I.; Arciola, C. R.; Fortunati, E.; Ferrari, D.; Mattioli, S.; Amoroso, C. F.;
382 Rizzo, J.; Kenny, J. M.; Imbriani, M.; Visai, L., The interaction of bacteria with engineered
383 nanostructured polymeric materials: a review. *TheScientificWorldJournal* **2014**, *2014*, 410423-
384 410423. DOI: 10.1155/2014/410423.
- 385 12. Chao, Y.; Liang, C.; Yang, Y.; Wang, G.; Maiti, D.; Tian, L.; Wang, F.; Pan, W.; Wu,
386 S.; Yang, K.; Liu, Z., Highly Effective Radioisotope Cancer Therapy with a Non-Therapeutic
387 Isotope Delivered and Sensitized by Nanoscale Coordination Polymers. *ACS Nano* **2018**, *12*
388 (8), 7519-7528. DOI: 10.1021/acsnano.8b02400.
- 389 13. Yang, Y.; Xu, L.; Zhu, W.; Feng, L.; Liu, J.; Chen, Q.; Dong, Z.; Zhao, J.; Liu, Z.; Chen,
390 M., One-pot synthesis of pH-responsive charge-switchable PEGylated nanoscale coordination
391 polymers for improved cancer therapy. *Biomaterials* **2018**, *156*, 121-133. DOI:
392 <https://doi.org/10.1016/j.biomaterials.2017.11.038>.
- 393 14. Liu, Y. L.; Tang, Z. Y., Multifunctional Nanoparticle@MOF Core-Shell Nanostructures.
394 *Adv. Mater.* **2013**, *25* (40), 5819-5825. DOI: 10.1002/adma.201302781.
- 395 15. Li, Y. T.; Tang, J. L.; He, L. C.; Liu, Y.; Liu, Y. L.; Chen, C. Y.; Tang, Z. Y., Core-
396 Shell Upconversion Nanoparticle@Metal-Organic Framework Nanoprobes for
397 Luminescent/Magnetic Dual-Mode Targeted Imaging. *Adv. Mater.* **2015**, *27* (27), 4075-4080.
398 DOI: 10.1002/adma.201501779.
- 399 16. Fan, X.; Yang, F.; Nie, C. X.; Yang, Y.; Ji, H. F.; He, C.; Cheng, C.; Zhao, C. S., Mussel-
400 Inspired Synthesis of NIR-Responsive and Biocompatible Ag-Graphene 2D Nanoagents for
401 Versatile Bacterial Disinfections. *ACS Appl. Mater. Interfaces* **2018**, *10* (1), 296-307. DOI:
402 10.1021/acsnano.7b16283.

- 403 17. Furukawa, H.; Cordova, K. E.; O’Keeffe, M.; Yaghi, O. M., The Chemistry and
404 Applications of Metal-Organic Frameworks. *Science* **2013**, *341* (6149), 1230444. DOI:
405 10.1126/science.1230444.
- 406 18. Zhao, M.; Yuan, K.; Wang, Y.; Li, G.; Guo, J.; Gu, L.; Hu, W.; Zhao, H.; Tang, Z.,
407 Metal–organic frameworks as selectivity regulators for hydrogenation reactions. *Nature* **2016**,
408 *539*, 76. DOI: 10.1038/nature19763
409 <https://www.nature.com/articles/nature19763#supplementary-information>.
- 410 19. Lu, K.; Aung, T.; Guo, N.; Weichselbaum, R.; Lin, W., Nanoscale Metal–Organic
411 Frameworks for Therapeutic, Imaging, and Sensing Applications. *Adv. Mater.* **2018**, *30* (37),
412 1707634. DOI: 10.1002/adma.201707634.
- 413 20. Lin, S.; Liu, X.; Tan, L.; Cui, Z.; Yang, X.; Yeung, K. W. K.; Pan, H.; Wu, S., Porous
414 Iron-Carboxylate Metal–Organic Framework: A Novel Bioplatfrom with Sustained
415 Antibacterial Efficacy and Nontoxicity. *ACS Appl. Mater. Interfaces* **2017**, *9* (22), 19248-19257.
416 DOI: 10.1021/acsami.7b04810.
- 417 21. Yuan, Y.; Wu, H.; Lu, H.; Zheng, Y.; Ying, J. Y.; Zhang, Y., ZIF nano-dagger coated
418 gauze for antibiotic-free wound dressing. *Chem. Commun.* **2019**, *55* (5), 699-702. DOI:
419 10.1039/C8CC08568D.
- 420 22. Song, Z.; Wu, Y.; Cao, Q.; Wang, H.; Wang, X.; Han, H., pH-Responsive, Light-
421 Triggered on-Demand Antibiotic Release from Functional Metal–Organic Framework for
422 Bacterial Infection Combination Therapy. *Adv. Funct. Mater.* **2018**, *28* (23), 1800011. DOI:
423 10.1002/adfm.201800011.
- 424 23. Mao, D.; Hu, F.; Kenry; Ji, S.; Wu, W.; Ding, D.; Kong, D.; Liu, B., Metal–Organic-
425 Framework-Assisted In Vivo Bacterial Metabolic Labeling and Precise Antibacterial Therapy.
426 *Adv. Mater.* **2018**, *30* (18), 1706831. DOI: 10.1002/adma.201706831.
- 427 24. Cui, D.; Huang, J. G.; Zhen, X.; Li, J. C.; Jiang, Y. Y.; Pu, K. Y., A Semiconducting
428 Polymer Nano-prodrug for Hypoxia-Activated Photodynamic Cancer Therapy. *Angew. Chem.*
429 *Inter. Ed.* **2019**, *58* (18), 5920-5924. DOI: 10.1002/anie.201814730.
- 430 25. Ng, C. W.; Li, J. C.; Pu, K. Y., Recent Progresses in Phototherapy-Synergized Cancer
431 Immunotherapy. *Adv. Funct. Mater.* **2018**, *28* (46). DOI: ARTN 1804688
432 10.1002/adfm.201804688.
- 433 26. Cui, D.; Xie, C.; Li, J. C.; Lyu, Y.; Pu, K. Y., Semiconducting Photosensitizer-
434 Incorporated Copolymers as Near-Infrared Afterglow Nanoagents for Tumor Imaging. *Adv.*
435 *Healthcare Mater.* **2018**, *7* (18). DOI:10.1002/adhm.201800329.
- 436 27. Ge, J.; Lan, M.; Zhou, B.; Liu, W.; Guo, L.; Wang, H.; Jia, Q.; Niu, G.; Huang, X.; Zhou,
437 H.; Meng, X.; Wang, P.; Lee, C.-S.; Zhang, W.; Han, X., A graphene quantum dot
438 photodynamic therapy agent with high singlet oxygen generation. *Nature Communications*
439 **2014**, *5*, 4596. DOI: 10.1038/ncomms5596
- 440 28. Chen, X. C.; Zhang, W., Diamond nanostructures for drug delivery, bioimaging, and
441 biosensing. *Chem. Soc. Rev.* **2017**, *46* (3), 27. DOI: 10.1039/C6CS00109B.
- 442 29. Ristic, B. Z.; Milenkovic, M. M.; Dakic, I. R.; Todorovic-Markovic, B. M.;
443 Milosavljevic, M. S.; Budimir, M. D.; Paunovic, V. G.; Dramicanin, M. D.; Markovic, Z. M.;
444 Trajkovic, V. S., Photodynamic antibacterial effect of graphene quantum dots. *Biomaterials*
445 **2014**, *35* (15), 4428-4435. DOI: <https://doi.org/10.1016/j.biomaterials.2014.02.014>.
- 446 30. Li, M.; Sultanbawa, Y.; Xu, Z. P.; Gu, W.; Chen, W.; Liu, J.; Qian, G., High and long-
447 term antibacterial activity against *Escherichia coli* via synergy between the antibiotic penicillin
448 G and its carrier ZnAl layered double hydroxide. *Colloids Surf. B: Biointerfaces* **2019**, *174*,
449 435-442. DOI: <https://doi.org/10.1016/j.colsurfb.2018.11.035>.
- 450 31. Song, H.; Ahmad Nor, Y.; Yu, M.; Yang, Y.; Zhang, J.; Zhang, H.; Xu, C.; Mitter, N.;
451 Yu, C., Silica Nanopollens Enhance Adhesion for Long-Term Bacterial Inhibition. *J. Am. Chem.*
452 *Soc.* **2016**, *138* (20), 6455-6462. DOI: 10.1021/jacs.6b00243.

- 453 32. Yue, Q.; Zhang, Y.; Jiang, Y.; Li, J.; Zhang, H.; Yu, C.; Elzatahry, A. A.; Alghamdi,
454 A.; Deng, Y.; Zhao, D., Nanoengineering of Core–Shell Magnetic Mesoporous Microspheres
455 with Tunable Surface Roughness. *J. Am. Chem. Soc.* **2017**, *139* (13), 4954-4961. DOI:
456 10.1021/jacs.7b01464.
- 457 33. Xu, R.; Huang, L.; Wei, W.; Chen, X.; Zhang, X.; Zhang, X., Real-time imaging and
458 tracking of ultrastable organic dye nanoparticles in living cells. *Biomaterials* **2016**, *93*, 38-47.
459 DOI: <https://doi.org/10.1016/j.biomaterials.2016.03.045>.
- 460 34. Yan, L.; Chen, X. F.; Wane, Z. G.; Zhang, X. J.; Zhu, X. Y.; Zhou, M. J.; Chen, W.;
461 Huang, L. B.; Roy, V. A. L.; Yu, P. K. N.; Zhu, G. Y.; Zhang, W. J., Size Controllable and
462 Surface Tunable Zeolitic Imidazolate Framework-8-Poly(acrylic acid sodium salt)
463 Nanocomposites for pH Responsive Drug Release and Enhanced in Vivo Cancer Treatment.
464 *ACS Appl. Mater. Interfaces* **2017**, *9* (38), 32990-33000. DOI: 10.1021/acsami.7b10064.
- 465 35. Ren, H.; Zhang, L. Y.; An, J. P.; Wang, T. T.; Li, L.; Si, X. Y.; He, L.; Wu, X. T.; Wang,
466 C. G.; Su, Z. M., Polyacrylic acid@zeolitic imidazolate framework-8 nanoparticles with
467 ultrahigh drug loading capability for pH-sensitive drug release. *Chem. Commun.* **2014**, *50* (8),
468 1000-1002. DOI: 10.1039/c3cc47666a.
- 469 36. Basavraj, S. N.; Namdev, M. S.; Bharat, W.; Sohan, S., Acidic Environment and Wound
470 Healing: A Review. *Wounds*. **2015**, *27* (1), 5-11.
471
472
473